AGU ADVANCING EARTH AND SPACE SCIENCES

Earth's Future

RESEARCH ARTICLE
10.1029/2024EF004825

# Constrained Precipitation Extremes Reveal Unequal Future Socioeconomic Exposure

**Ziyi Liu[1], Yao Yue[1,2,3], Louise Slater[4], Alistair G. L. Borthwick[5,6], Yuanfang Chai[7], Xiaofan Luan[8,9], Chiyuan Miao[7], and Zhonghua Yang[1]**

[1]State Key Laboratory of Water Resources Engineering and Management, School of Water Resources and Hydropower Engineering, Wuhan University, Wuhan, China, [2]Institute for Water-Carbon Cycles & Carbon Neutrality, Wuhan University, Wuhan, China, [3]State Key Laboratory of Hydraulics and Mountain River Engineering, Sichuan University, Chengdu, China, [4]School of Geography and the Environment, University of Oxford, Oxford, UK, [5]Institute for Infrastructure and Environment, School of Engineering, The University of Edinburgh, Edinburgh, UK, [6]School of Engineering, Mathematics and Computing, University of Plymouth, Plymouth, UK, [7]State Key Laboratory of Earth Surface Processes and Resource Ecology, Faculty of Geographical Science, Beijing Normal University, Beijing, China, [8]School of Urban Design, Wuhan University, Wuhan, China, [9]Hubei Habitat Environment Research Center of Engineering and Technology, Wuhan, China

**Key Points:**

- A new emergent constraint relationship is proposed which reduces uncertainty in extreme precipitation projections by CMIP6 models
- Future population and GDP exposure to extreme precipitation is expected to increase, driven by climatic and coupled socio-economic factors
- Most high-risk countries are socio-economically vulnerable, politically unstable, with low-income, and may be self-perpetuating

**Supporting Information:**

Supporting Information may be found in the online version of this article.

**Correspondence to:**

Y. Yue,
yueyao@whu.edu.cn

**Citation:**

Liu, Z., Yue, Y., Slater, L., Borthwick, A. G. L., Chai, Y., Luan, X., et al. (2024). Constrained precipitation extremes reveal unequal future socioeconomic exposure. *Earth's Future*, *12*, e2024EF004825. https://doi.org/10.1029/2024EF004825

Received 20 APR 2024
Accepted 12 NOV 2024



**Abstract** Extreme precipitation can lead to major flooding, impacting human health and safety. Thus, reliable projections of population and GDP exposure to future extreme precipitation are imperative. Here, we quantify future precipitation characteristics from robust emergent constraint relationships between historical and future monthly precipitation extremes (99th percentile) across 19 CMIP6 models ($r^2 > 0.7$ in 74–84% of 0.5° global land grids), and narrow uncertainty by 37.0–39.5% (absolute reduction being 0.753–0.774 mm/day). The constrained grid-averaged future 99th percentile extreme is 6.96 ± 0.0059, 7.03 ± 0.0061, 7.11 ± 0.0063, and 7.29 ± 0.0067 mm/day, under SSP126, SSP245, SSP370, and SSP585, respectively, which exceeds historical extremes substantially in terms of intensity (12.9–19.7%) and frequency (1.6–2.3 times more). Future population and GDP exposed to 99th percentile extreme precipitation grow quickly, and are projected to exceed 1 million people in 27–40 countries and 10 billion USD (2005 Purchasing-Power Parity) in 48–77 countries. Growth of future population exposure is dominated by an increase in extreme precipitation frequency rather than a rise in population, especially in developed countries. GDP exposure is controlled by the coupled effects of rapid socio-economic development and significant shifts in precipitation frequency. Using indices of socio-economic vulnerability, government effectiveness and economic freedom, we identify the unequal situation that high-risk countries with high exposure are commonly characterized by low GDP per capita and high sociopolitical instability.

**Plain Language Summary** Extremely heavy precipitation poses a substantial threat to human lives, wellbeing, and property, particularly in disadvantaged countries. To better understand the future risk due to exposure to extreme precipitation, we propose a new relationship, the "emergent constraint" between historical simulations and future projections from climate models. This relationship allows us to provide more accurate projections of extreme precipitation with 99th percentile. These improved estimates show that future extreme precipitation is expected to surpass historical levels in both intensity and frequency. Thus, more than 1 million people in 27–40 countries, notably in China and India, could be threatened, and over 10 billion USD of GDP (2005 Purchasing-Power Parity) could be wiped out in 48–77 countries. The increase in population exposure to extreme precipitation is primarily driven by a rise in the frequency of the extreme events, while the rising exposure of GDP results from both socio-economic development and shifts in extreme frequency. Notably, the high-risk countries stand out due to their sociopolitical instability and typically low GDP per capita, which may lead to a self-perpetuating situation due to the incapability to cope with the risk.

## 1. Introduction

Extreme precipitation can lead to significant human and property losses, especially in countries ill-equipped to manage such risks (de Bruijn et al., 2019; De Silva et al., 2018; Hallegatte et al., 2016; Rentschler et al., 2022; Tanoue et al., 2016). For instance, the recent Storm Daniel disaster in Libya killed nearly 4,000 people, with 9,000 unaccounted for, dealing a severe blow to a country that has been entrenched in political crisis (https://www.emro.who.int/lby/floods/index.html). Future projections show that both the frequency and intensity of extreme precipitation are likely to increase in the context of climate change (Chen et al., 2020; Gu et al., 2023;

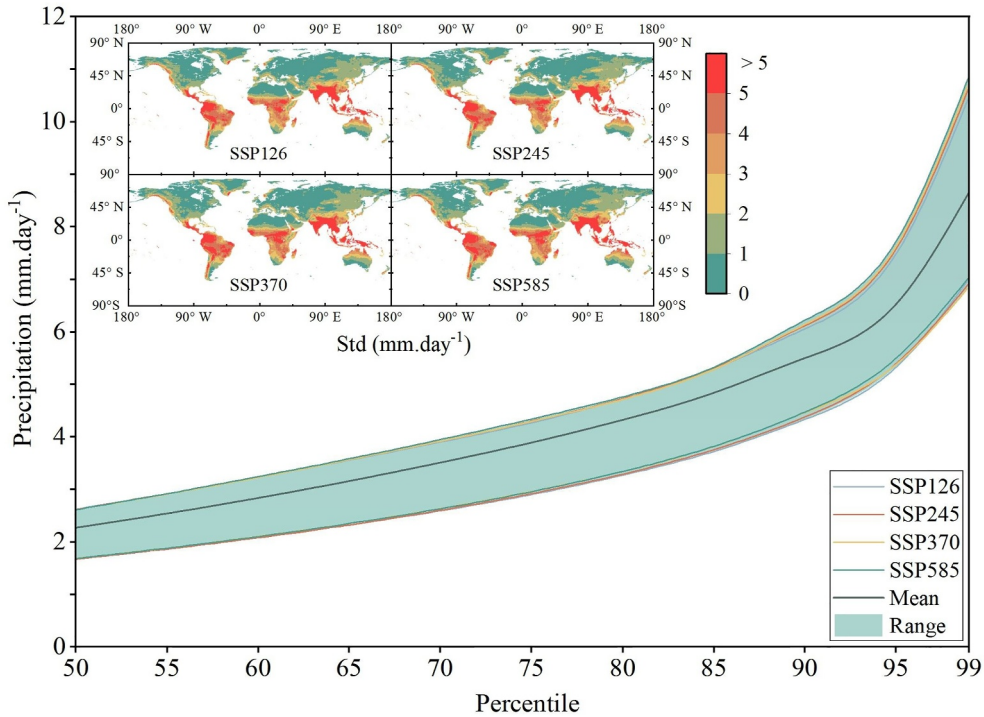


**Figure 1.** Range of projected global-average 50th–99th percentiles of monthly precipitation from 19 CMIP6 models. Inset maps in the top left corner represent the standard deviation spatial distribution of the projected 99th percentile of precipitation across the models under the SSP126, SSP245, SSP370 and SSP585 shared socioeconomic pathways.

Papalexiou & Montanari, 2019; Sohn et al., 2019; Zhang et al., 2018). Meanwhile, ongoing population growth and economic development can increase exposure to risk, especially in underdeveloped regions (IMF, 2023; UN DESA, 2022). Therefore, it is essential to assess the risks associated with future extreme precipitation in the context of population growth and economic development, and hence identify the most vulnerable regions.

Accurate projections of the future frequency and intensity of extreme precipitation provide the basis for risk assessment. However, considerable uncertainty exists in General Circulation Model (GCM) projections of future precipitation, especially for extremes. As shown in Figure 1 which is based on global mean and the spread across 19 CMIP6 models, the range (width of the light cyan shadow) for the projected precipitation intensity of 99th percentile (3.5–3.9 mm/day under four SSPs) is nearly four times as the range for 50th percentile (0.93–0.95 mm/day). Besides, the change in the mean intensity of the 19 models from 50th percentile to 99th percentile (roughly 6 mm/day) over the range of 99th percentile (roughly 4 mm/day), which represents the ratio of signal to noise, is 1.5. The Emergent Constraint is an effective method to reduce the uncertainty of GCM projections (Brient, 2020; Hall et al., 2019; Williamson et al., 2021). Notably, Thackeray et al. (2022) and Zhang et al. (2022) established emergent constraints for extreme precipitation, and effectively reduced the projection uncertainty by 20–40% ($r^2$ is between 0.36 and 0.71). However, there is still room to constrain uncertainty further by proposing more robust emergent constraint relationships.

Another key issue for assessing risk and vulnerability is the selection of proper indicators for risk exposure and disaster resilience. The mortality rate and the economic loss caused by disasters are commonly used indicators for estimating risk. For example, Forzieri et al. (2017) used annual deaths and the exposed population as indicators to assess future impacts of weather-related risk in Europe. Shi et al. (2016) established a model that couples hazard intensity with vulnerability to estimate annual risk from various climate disasters in terms of global expected mortality rate, affected population rate, and GDP loss rate. Dottori et al. (2018) calculated future global deaths and direct economic losses resulting from river flood events at various warming levels. The total number of people and the social wealth that are potentially affected (under all possible pathways) are often calculated in terms of total population and GDP of the region (Chen et al., 2020; Chen & Sun, 2021; Das et al., 2022; Liu et al., 2020; Shen et al., 2022). Multiple indicators are used to estimate the vulnerability of a country, including government

efficiency and effectiveness, infrastructure, population, income, education, health, gender, and age (Brooks et al., 2005; Cutter et al., 2003; Fatemi et al., 2017; Karunarathne & Lee, 2020; Mesta et al., 2020; Rufat et al., 2015).

This paper aims to develop a robust emergent constraint relationship to improve the projection of future frequencies and intensities of extreme precipitation (99th percentile) and reduce their uncertainty. Changes in the total number of people exposed and the social wealth potentially affected are then quantified for each country in the world. Dominant drivers (i.e., factors that account for the largest proportion of the changed exposure) for these changes are analyzed. Finally, high-risk areas that are most vulnerable and lack the ability to cope with flood-related disasters are identified and the unequal impacts of precipitation extremes examined. The advance of our study is that it makes the first attempt to combine the emergent constraint on precipitation with its socio-economic impacts (i.e., on GDP and population), providing insights into future population and GDP exposures based on estimates of extreme precipitation with less uncertainty.

## 2. Materials and Methods

### 2.1. Earth System Models and Observation Data Sets for Deriving the 99th Percentile Precipitation

Earth system models (ESMs) serve as critical tools for advancing our understanding of the Earth's complex interactive processes, enabling the projection of future climate scenarios, and informing policy decisions to mitigate and adapt to climate change. CMIP6 and CMIP5 represent the 6th and 5th generation of these models within the Coupled Model Intercomparison Project, respectively. We use 19 models (full names listed in Table S1 in Supporting Information S1) of monthly precipitation from CMIP6 (Coupled Model Intercomparison Project Phase 6) over the historical (1980–2014) and future (2015–2100) periods under four different emission scenarios (i.e., SSP126, SSP245, SSP370 and SSP585), and 17 models from CMIP5 (Coupled Model Inter-comparison Project Phase 5) over the 1900–2005 and 2006–2100 periods under three different representative concentration pathways (RCP2.6, RCP4.5 and RCP8.5) for an out-of-sample test. Additionally, we use five present-day precipitation data sets: CMAP (Xie & Arkin, 1997), CPC (Chen et al., 2008; Xie et al., 2007), GPCC (Schneider et al., 2015), MSWEP2 (Beck et al., 2019), and PRECL (Chen et al., 2002) as the observational constraint in our hierarchical emergent constraint framework.

The 99th percentile delineates a value which is equal to or greater than 99% of all the data points in a set, with the remaining 1% exceeding this value. This concept is frequently employed to characterize the occurrence of rare or extreme events in the fields of hydrology and meteorology (Murray & Ebi, 2012; Thackeray, 2022; Wilks, 2011). Here we utilized the above data sources to obtain the monthly precipitation data of 420 months in the history from 1980 to 2014 (both observed and simulated), and of 1032 months in the future from 2015 to 2100 to determine 99th percentiles, for the historical and future periods, respectively.

It should be noted that floods occur when heavy rainfall over saturated river catchments generates streamflow rates that exceed the local river channel conveyance capacity, and such high streamflow magnitudes occur when river catchments are saturated following heavy rainfall over many days. The impact on people affected by the flood lasts even longer. Given that the focus of this study is on the impacts of extreme precipitation on population and GDP, we use monthly precipitation data instead of daily data, even if the peak process in the flood hydrograph covers a short timescale. Using the monthly timestep data can be further justified by the following fact: if the precipitation in a single month falls within the 99th percentile, it is highly probable that the 99th percentile of daily precipitation will also occur during this month (see Table S2 in Supporting Information S1).

Noting that the precipitation data from the models and observational sets should first be re-gridded globally at $0.5° \times 0.5°$ latitude-longitude spatial resolution using bilinear interpolation to generate uniform grids. Then 99th percentiles are calculated for each grid using the above method. Thus, we can avoid direct bilinear interpolation for extreme values.

### 2.2. Hierarchical Emergent Constraint Method

Hierarchical Emergent Constraint (HEC) are a multi-tiered statistical approach that enhances the prediction of climate responses by integrating emergent relationship between future and current climate states with observations, surpassing Emergent Constraints (EC) that do not consider observational uncertainty. We employ a hierarchical emergent constraint framework from Bowman et al. (2018) to reduce the uncertainty of future

precipitation projections from the CMIP6 models. The least squares linear regression method is used to develop emergent relationships between $x$ and $y$ (Equation 1) in each 0.5° × 0.5° latitude-longitude grid cell,

$$y = k(x - \overline{x}) + \overline{y} \tag{1}$$

where $x$ is the simulated historical extreme precipitation in all the selected CMIP6 models and $y$ is the projected future extreme precipitation; $\overline{y}$ and $\overline{x}$ are the multi-model ensemble mean values of $y$ and $x$; $k$ is the slope of the regression equation. Under a Gaussian assumption, the expected value of the constrained future extreme precipitation, $\overline{y}_c$, and its standard deviation, $\sigma_{y_c}$, are primarily influenced by the Signal-to-Noise Ratio (*SNR*) and the correlation coefficient ($\rho$) between $x$ and $y$. *SNR* defines the relative strength of the signal variability to the noise variability,

$$SNR = \frac{\sigma_{x_t}^2}{\sigma_{x_0}^2} \tag{2}$$

where $\sigma_{x_t}^2$ is the variance of the historical extreme precipitation simulations of the CMIP6 models and $\sigma_{x_0}^2$ is the variance of the selected observational data sets. If the signal overwhelms the noise, then the effect of the constraint is determined principally by $\rho$. Conversely, when the noise dominates, the variance reduction rate of the raw projections will be close to 0. $\overline{y}_c$ and $\sigma_{y_c}$ can be derived from

$$\overline{y}_c = \overline{y} + \frac{\rho \frac{\sigma_y}{\sigma_x}}{1 + SNR^{-1}}(\overline{x}_0 - \overline{x}) \tag{3}$$

$$\sigma_{y_c}^2 = \left(1 - \frac{\rho^2}{1 + SNR^{-1}}\right)\sigma_y^2 \tag{4}$$

where $\overline{x}_0$ is the mean value of the selected historical observed extreme precipitation and $\sigma_y$ is the inter-model standard deviation of $y$.

It should be noted that Bowman et al.'s (2018) method is based on Gaussian assumption. According to previous studies, the occurrence of climate extremes over a long period of time is more likely to comply with the Generalized Extreme Value Distribution (Papalexiou & Koutsoyiannis, 2013) and the Gamma Distribution (Zhang et al., 2022) than the Gaussian distribution. Nevertheless, the parameters of this Gaussian process in Bowman et al.'s (2018) paper are "the mean and variance from the CMIP5 model ensemble", rather than the mean and variance over a time period. It is possible that the precipitation extremes from CMIP6 model ensemble would comply with the Gaussian distribution, because the CMIP6 models can be supposed to be independent of each other, and the mean value of a series of independent variables is likely to fit the Gaussian distribution according to the central-limit theorem.

Therefore, we drew the frequency histogram of the global mean 99th percentile from the 19 CMIP6 models to test the Gaussian hypothesis (Figure S1 in Supporting Information S1) and found that it cannot be denied. And also, the fitted Gaussian curve has a strong correlation with the original frequency distribution ($r^2$ = 0.962, *RMSE* = 0.0755). Then, we tested the Gaussian hypothesis for every grid, and cannot deny it in 99.26% of all the studied grids. There are also other studies which applied HEC based on Gaussian hypothesis to constrain the extreme precipitation (Thackeray et al., 2022; Zhang et al., 2022). For the occurrence of extreme precipitation over a long period, Zhang et al. (2022) explicitly assumed a Gamma distribution to explain the mechanism behind the emergent constraint relationship for precipitation extremes; then, they used the mean and variance of the CMIP5 model ensemble to set up an HEC method, which means the Gaussian distribution was implicitly assumed. It again implies that the distributions of a random variable over a time period and across CMIP6 models may be different, and the use of HEC in this study is reasonable. We also used the raw emergent constraint method which does not require a Gaussian distribution for the two climate variables in the remaining 0.74% grids which fit GEV distribution, and compared the results with those derived from the HEC method (see Text S1 and Figure S2 in Supporting Information S1).

### 2.3. Potential Exposure of Population and GDP to Risk of Extreme Precipitation

Here we adopt the statistical expectations of population and GDP that may be affected by extreme precipitation as measures of potential exposure (Chen et al., 2020; Chen & Sun, 2021; Das et al., 2022; Liu et al., 2020; Shen et al., 2022). Therefore, the changed potential exposure is:

$$\Delta E_{\text{Population}} = \frac{(F_h + \Delta F)(P_h + \Delta P) - F_h \times P_h}{F_h \times P_h} \tag{5}$$

$$\Delta E_{\text{GDP}} = \frac{(F_h + \Delta F)(F_h + \Delta \text{GDP}) - F_h \times \text{GDP}_h}{F_h \times \text{GDP}_h} \tag{6}$$

where $F$ is the frequency of occurrence of extreme precipitation; $P$ is the frequency of occurrence of population; and $\Delta$ is the changed value between the future and the historical periods.

To determine the frequency change ($\Delta F$) given the precipitation intensity of the historical 99th percentile, we also identified the emergent constraint relationships for 70th, 75th, 80th, 85th, 90th and 95th percentiles of precipitation, and acquired the constrained precipitation intensities for each of the percentiles in the future. Therefore, a future intensity versus percentile line chart can be drawn for each grid (the pink line in Figure S3 in Supporting Information S1). By applying the precipitation intensity of the historical 99th percentile (the horizontal dashed line in Figure S3 in Supporting Information S1), its corresponding constrained future percentile is obtained by linear interpolation (methods given in Supporting Text S2 in Supporting Information S1) in the line chart (the vertical dashed line in Figure S3 in Supporting Information S1). The change in frequency is the difference between 99 and the constrained future percentile.

The uncertainties for future exposures of population and GDP and for future frequency given the historical 99th percentile precipitation intensity can be derived by uncertainty propagation law using uncertainties in future projected precipitation intensities (Supporting Text S3 in Supporting Information S1).

Note that Equations 5 and 6 can be deformed into Equations 7 and 8 in which three potential drivers are identified for the changed exposure: increased frequency of extreme precipitation ($\Delta F/F_h$), increased population/GDP ($\Delta P/P_h$ or $\Delta\text{GDP}/\text{GDP}_h$) and coupled effects of increased frequency and population/GDP [$(\Delta F \times \Delta P)/(F_h \times P_h)$ or $(\Delta F \times \Delta\text{GDP})/(F_h \times \text{GDP}_h)$]:

$$\Delta E_{\text{Population}} = \frac{\Delta F}{F_h} + \frac{\Delta P}{P_h} + \frac{(\Delta F \times \Delta P)}{F_h \times \text{P}_h} \tag{7}$$

$$\Delta E_{\text{GDP}} = \frac{\Delta F}{F_h} + \frac{\Delta\text{GDP}}{\text{GDP}_h} + \frac{(\Delta F \times \Delta\text{GDP})}{F_h \times \text{GDP}_h} \tag{8}$$

This enables us to analyze the main driving factor that accounts for the largest proportion of the changed exposure among the three potential drivers in different countries.

World Bank Group provides population and GDP data for historical periods. The IIASA-WiC POP model (Samir & Lutz, 2017), developed by the International Institute for Applied Systems Analysis (IIASA), projects future population growth under various Shared Socioeconomic Pathways and aligns demographic assumptions with energy system and greenhouse gas trajectories. The OECD Env-Growth model (Dellink et al., 2017), developed by the Organization for Economic Cooperation and Development (OECD), projects long-term global economic growth within the SSP framework, forecasting GDP and income levels based on conditional convergence, where less developed countries are expected to grow faster than more developed ones.

Future national demographic data and GDP at purchasing power parity are derived using data at 5-year intervals from the IIASA-WiC POP model (Samir & Lutz, 2017) and the OECD Env-Growth model (Dellink et al., 2017) from the SSP Database, and averaged over a 75-year period from 2015 to 2100. Meanwhile, we select the historical population data every five years from 1980 to 2014 (including 2014) and calculate its mean value. The average GDP at purchasing power parity from 2000 to 2014 is used to represent the historical value of GDP for each country. Note that historical and future national GDP data may have different units, in which case it is necessary to convert them using the GDP Purchasing Power Parity Conversion Factor (PPP).

## 3. Main Results

### 3.1. Constrained Frequency and Intensity of Future Extreme Precipitation

To reduce uncertainty in the CMIP6 model projections, we employ the hierarchical emergent constraint (HEC) method, which integrates emergent relationships between historical and future intensities of 99th percentile precipitation extremes with five observational data sets ($SNR > 1$ across more than 76.5% of world's land surface). Mechanisms for the emergent constraint relationship is explained in Supporting Information (Figure S4 and Supporting Text S4 in Supporting Information S1). Figure S5 in Supporting Information S1 demonstrates the form of emergent relationship at the global scale, and we identified relationships in a similar form for every studied grid under four SSPs. Since the emergent relationship is linear, correlation coefficient ($r$) is used for testing the association of historical extreme precipitation and projected future extreme precipitation (Asuero et al., 2006). The statistical relationship is strong ($r^2 > 0.7$ in 74–84% of the grid cells) and remains strong for 84% of areas based on out-of-sample testing using 17 CMIP5 models (Figure S6 in Supporting Information S1). The constrained standard deviation is always smaller than the unconstrained distribution in each grid cell across all four SSPs, indicating that the confidence interval of the projected variable is confined within a narrower range and that the proposed HEC performs well in reducing the uncertainty of future projections at the grid cell scale (Hall et al., 2019). For the global mean, the decreased uncertainty in projected extreme precipitation is 37.0–39.5% (absolute reduction being 0.753–0.774 mm/day) under the four SSPs (Figure 2 and Figure S7 in Supporting Information S1). In particular, the uncertainty decreases by 60–80% (over 5 mm/day) in the near-equatorial region where the raw CMIP6 projections have wider ranges than in other regions (inset map of Figure 1), such as Southeast Asia, Central Africa, and South America (Figure S8 in Supporting Information S1). Compared to previous studies on emergent constraints for extreme precipitation events (Thackeray et al., 2022; Zhang et al., 2022), the proposed statistical relationship demonstrates improved performance. Specifically, the grid-averaged correlation ($r^2$) ranges from 0.785 to 0.832 under four SSPs, while the $r^2$ of the emergent constraint relationships for the globally averaged extreme precipitation at the 99th pertcentile spans from 0.906 to 0.957 (see Figure S5 in Supporting Information S1). These values exceed the maximum globally averaged $r^2$ of 0.71 reported by Thackeray et al. (2022). In terms of global distribution, the most significant correlations are observed in the extratropics in Zhang et al. (2022), with $r^2$ values exceeding 0.36 at the grid point scale across most regions. Notably, our analysis reveals that $r^2$exceeds 0.7 in over 74% of the regions (see Figure 2).

The constrained grid-averaged future 99th percentile extreme is 6.96 ± 0.0059 mm/day under SSP126, 7.03 ± 0.0061 mm/day under SSP245, 7.11 ± 0.0063 mm/day under SSP370, 7.29 ± 0.0067 mm/day under SSP585, compared with the raw projections of 7.70 ± 0.0113 mm/day, 7.78 ± 0.0115 mm/day, 7.87 ± 0.0117 mm/day, and 8.05 ± 0.0120 mm/day, from SSP126 to SSP585. Comparisons with raw projections from each of the 19 models are summarized in Table S3 in Supporting Information S1. Using the constrained precipitation projections, we examine projected future variations in both intensity and frequency of the 99th percentile extremes across SSP126, SSP245, SSP370, and SSP585. In 46–63% of the grid cells, the increase in intensity is more than 10% and the shift in frequency is greater than 135% (i.e., 1.35 times higher) compared with the historical 99th percentile extreme. These grid cells are identified as rapidly changing. Extreme intensities at 99th percentile in the historical period are even projected to be at the 95th percentile in the future period under SSP585 in countries such as Iceland, Somalia, Somaliland, and Tajikistan. Notably, we find that the raw CMIP6 projections overstate the associated hazards of extreme precipitation intensity (by 15.8–16.1%, summarized from Figure S9 in Supporting Information S1) and frequency (by 234–249%, summarized from Figure 2). The percentage of the rapidly changing grids is also overestimated by the raw CMIP6 projections (in 67–73% of the grid cells).

### 3.2. Changes in Exposure and the Primary Drivers

We estimate future exposure by multiplying the total population or GDP of a nation by the projected frequencies of constrained extreme precipitation. Exposure reflects the overall population or societal wealth that would be threatened by the hazard of extreme precipitation. In the future period (2015–2100), the average likely population exposed to 99th percentile precipitation is projected to surpass 1 million (at 95% confidence level, i.e. $\mu - 1.65\sigma \geq 1$ million) in 27–40 countries and GDP exposure is found to reach 10 billion USD (at 95% confidence level, i.e. $\mu - 1.65\sigma \geq 10$ billion USD, 2005PPP) in 48–77 countries (see Figure 3; $\mu$ and $\sigma$ are given in Tables S4–S7 in Supporting Information S1) summarized from outcomes of four SSPs. Notably, population exposure

10.1029/2024EF004825

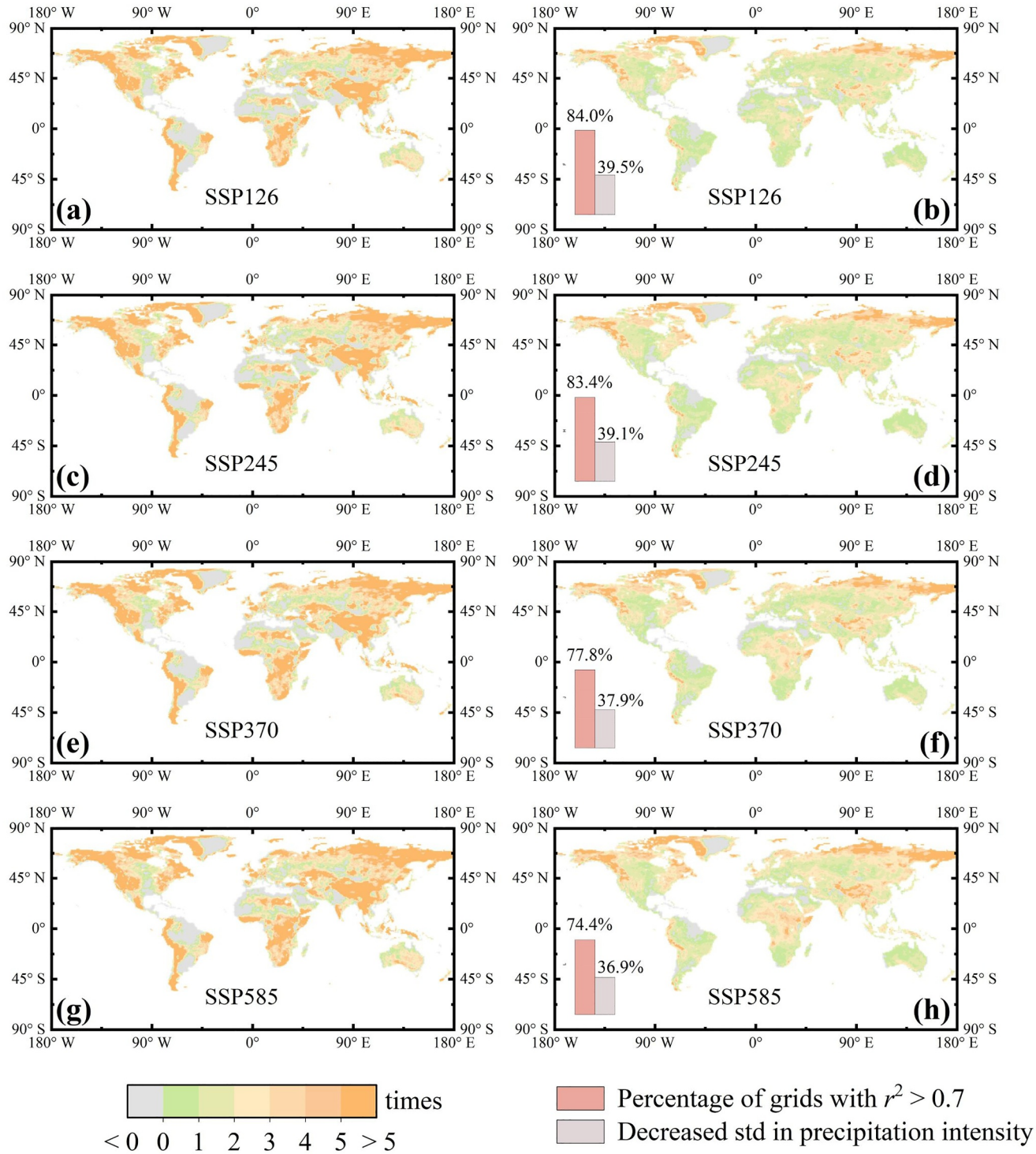


**Figure 2.** Changes in future frequency of occurrence of historical 99th percentile extreme precipitation at grid scale under the four SSPs before (a), (c), (e), and (g) and after (b), (d), (f), and (h) application of the emergent constraint. Frequency changes are shown as growth multiples. Pink bars represent the percentage of grid cells with a coefficient of determination ($r^2$) greater than 0.7 for the emergent constraint relationships identified across 19 CMIP6 models; light purple bars indicate the reduction in mean standard deviation for constrained intensity of 99th percentile precipitation after emergent constraint.

may even over 30 million in countries that are heavily populated, such as China (32.3 ± 0.7–42.1 ± 0.9 million) and India (31.5 ± 2.1–54.2 ± 2.8 million). Future GDP exposures (billion USD, 2005PPP) of China (1126.8 ± 24.8–2930.5 ± 64.3), France (66.2 ± 7.4–187.5 ± 19.6), Germany (80.3 ± 6.0–229.1 ± 14.3), India

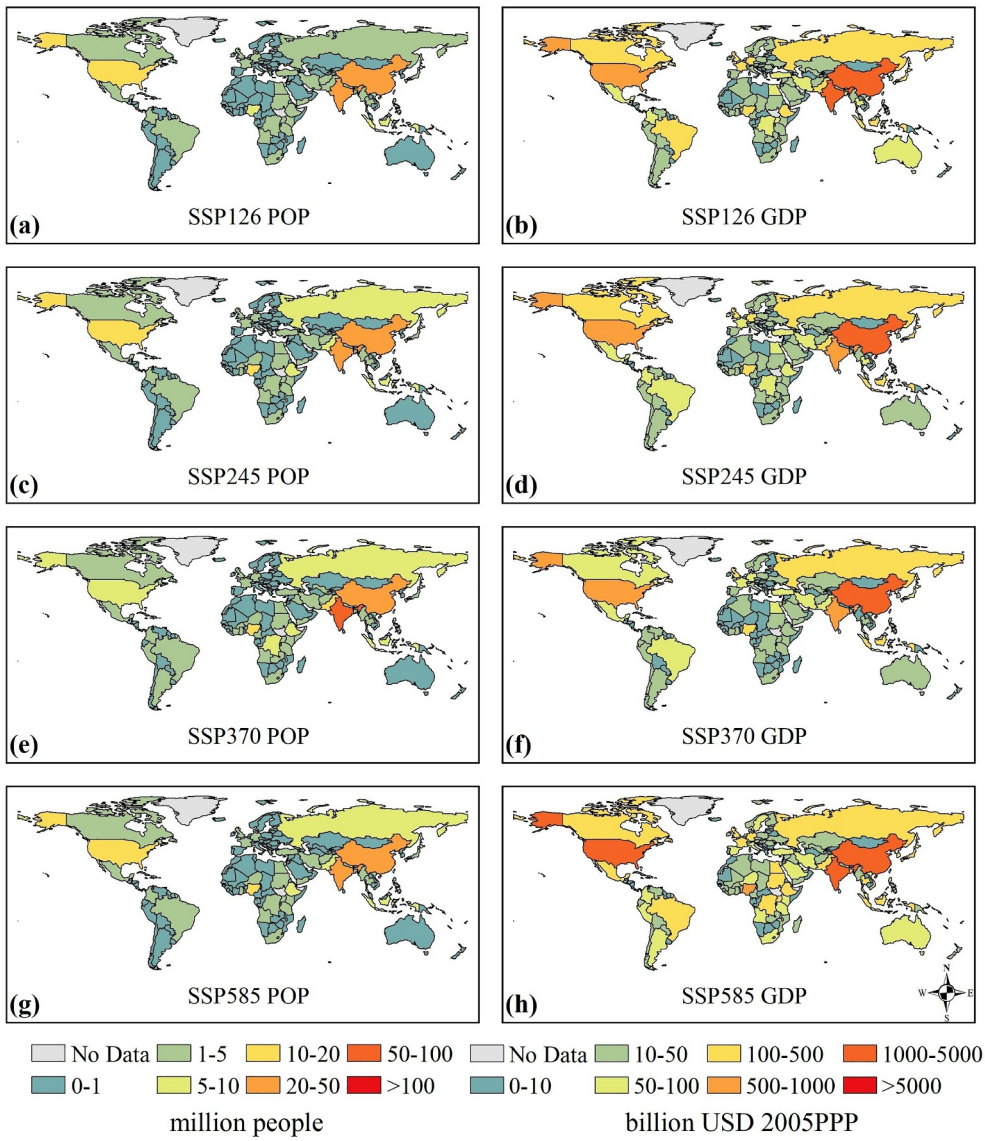


**Figure 3.** The expectation of future population (a), (c), (e), and (g) and GDP (b), (d), (f), and (h) exposed to 99th percentile extreme precipitation at grid scale under the four SSPs after application of the emergent constraint.

(568.8 ± 29.3–2090.9 ± 93.5), the United Kingdom (106.4 ± 12.2–349.9 ± 34.8), and the United States (614.3 ± 13.9–1829.0 ± 38.3) surpass all other countries by far (Tables S4–S7 in Supporting Information S1).

Figure 4 and Figures S9–S11 in Supporting Information S1 display the projected population and GDP exposure changes worldwide for different SSPs over the future period (2015–2100). The population exposure of 103–115 countries, is projected to surge by over 100% in the future period. Meanwhile, the future GDP exposure of 87–120 countries is projected to exceed five times their historical exposure due to rapid economic expansion under the four SSPs. The projected changes in exposure could exceed a fivefold increase in population and a twentyfold increase in GDP under all four SSPs in Afghanistan, Burkina Faso, Burundi, DR Congo, Ethiopia, Liberia, Malawi, Niger, Nigeria, Rwanda, and Uganda, all of which are located in ither Africa or Asia.

Changes in exposure can be driven by shifts in the frequency of extreme precipitation, growth of population, growth of GDP, or the coupled effects of both population and GDP (see Methods). Amplified by 84–287%, the climate change factor (i.e., $\Delta F/F_h$ in Equation 7) is identified as the major driver of future population exposure for all continents (e.g., contributing 26–96% under SSP245, see Figure 4, other SSPs see Figures S10–S12 in

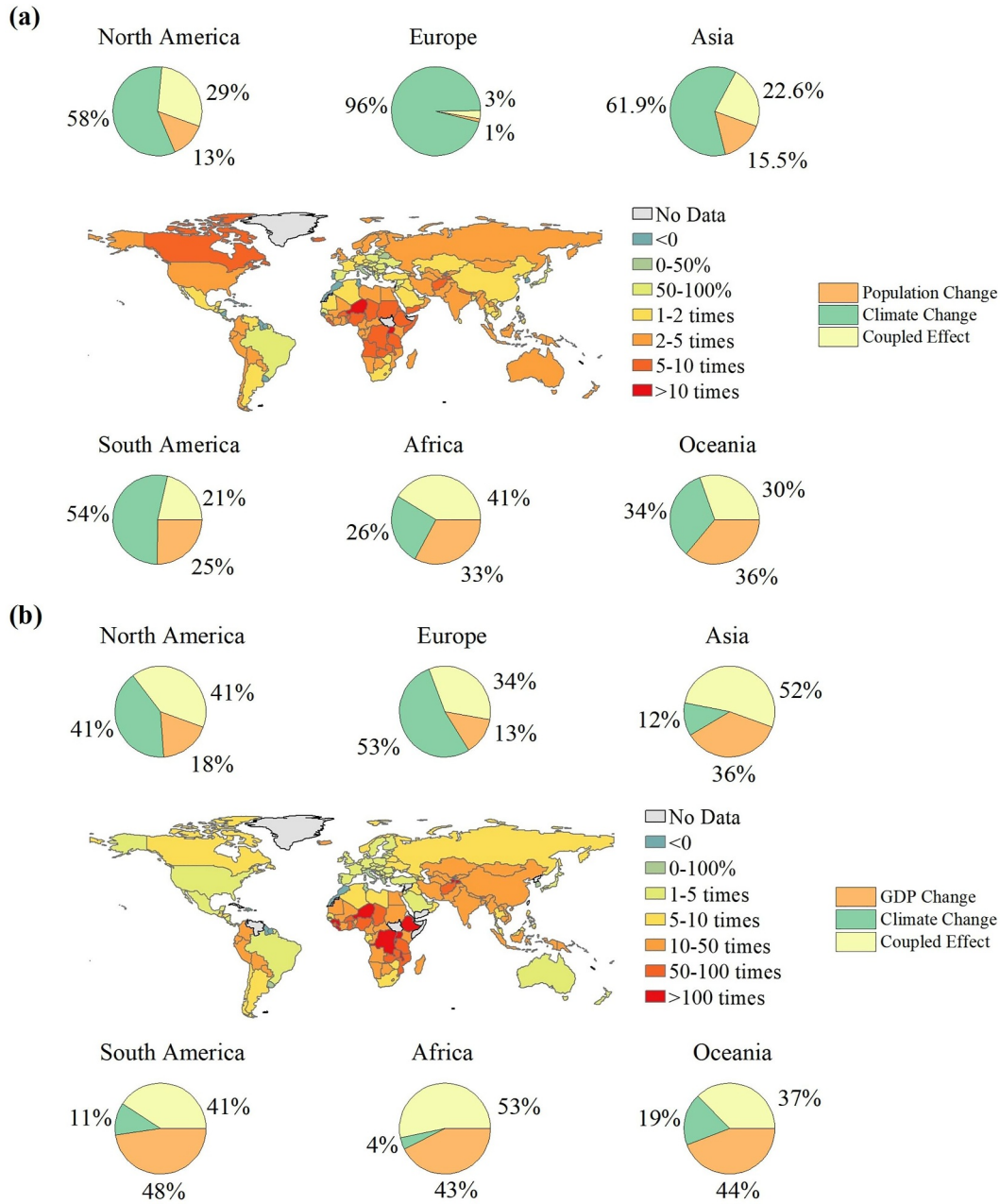


**Figure 4.** Future relative changes (expressed as growth multiples when exceeding 100%) in total population (a) and GDP (b) exposure to the historical 99th percentile of precipitation extremes under SSP245 for each country. The six inset pie charts depict the contribution of each driver to the relative changes for each of the six continents; the contributions are derived from the increase in population/GDP, shift in extreme precipitation frequency, and combined effect of socio-economic development and climate change.

Supporting Information S1) except Africa. Climate impact becomes increasingly pronounced as the future carbon emission level gradually increases from SSP126 to SSP585. In Europe, the climate change factor is projected to account for over 95% of the exposure under SSP126, SSP245, and SSP370. In Africa, the coupled effect of population increase and climate change (i.e., $(\Delta F \times \Delta P)/(F_h \times P_h)$ in Equation 7) is the leading driver (35–48% under the four SSPs). Although the global population growth rate is expected to gradually stabilize or even become negative in certain regions in the future, African countries continue to exhibit substantial population growth. Therefore, the sole effect of population growth (i.e., $\Delta P/P_h$ in Equation 7) is important in Africa, contributing 23–34% to population exposure across the four SSPs. Interestingly, the population changes peak in

the SSP3 scenario and reach a minimum in the SSP5 scenario in continents containing a significant number of developing countries, such as Asia, Africa, and South America, whereas Europe, North America, and Oceania exhibit the opposite trend. The population patterns explain the different roles of population change under the four SSPs.

The main driver for the change in GDP exposure is the coupled effect of the shift in extreme precipitation frequency and GDP growth (i.e., $(\Delta F \times \Delta \mathrm{GDP})/(F_h \times GDP_h)$ in Equation 8) for Asia, Africa, and South America under the four SSPs (e.g., contributing 41–53% under SSP245, see Figure 4, other SSPs see Figures S10–S12 in Supporting Information S1). North America and Oceania exhibit a similar pattern, exception under the SSP370 scenario due to a relative slowdown in GDP growth. In Europe however, rapid economic growth is unlikely to replace the dominant role of climate change (i.e., $\Delta F/F_h$ in Equation 8), except under the SSP585 scenario in which coupled effects are expected to completely take the lead. Unlike demographic change, GDP changes in each continent are projected to decrease gradually from SSP1 to SSP3 but increase to the highest level under SSP5. Among the 11 low-income countries with GDP per capita below 750.5 USD in 2022 (Population and GDP data, 2022), the changes in population exposure in 6–9 countries (Burundi, DR Congo, Mozambique, Malawi, and Yemen under all SSPs) and the changes in GDP exposure in 7–8 countries (Burundi, Central African Republic, DR Congo, Mozambique, Malawi, and Sierra Leone under all SSPs) are primarily dominated by the coupled effects (i.e., climate change coupled with population or GDP changes under the four SSPs). The absence of historical GDP data records precludes an analysis of GDP exposure fluctuations. in Yemen and Somalia.

## 4. Discussion

### 4.1. Frequency Shift of Heavy Precipitation at the 70th–95th Percentiles

With relatively higher intensities, heavy precipitation events could inflict significant socioeconomic pressure on countries characterized by political and social unrest or lower resilience to natural disasters. We estimate the mean change in intensity of heavy precipitation at the 70th–95th percentiles for each continent (averaged over grids) from the shift in the entire probability distribution based on constrained projections (Figure S13 in Supporting Information S1) and give the uncertainties in Tables S8–S14 in Supporting Information S1 using the uncertainty propagation law (Supporting Text S3 in Supporting Information S1). For heavy precipitation, the raw CMIP6 models overestimate future changes compared to the constrained result, but the relative overestimation is less than that for 99th percentile of extreme precipitation (Figure S13 in Supporting Information S1). Although the greatest intensity of heavy precipitation at the 70th–95th percentile is projected to occur in South America, the corresponding change in intensity is relatively small (−0.7–6.7% under the four SSPs). In contrast, Europe displays lower intensity, but the changes are expected to be the largest (14.7–21.9% under the four SSPs) in the future. One notable exception is that the 70th percentile of precipitation in South America is expected to decrease under SSP370 and SSP585. Meanwhile, heavy precipitation at the same intensity level is projected to occur more frequently in the future period than in the historical period. Under SSP245, the frequency of the historical 70th to 95th percentile precipitation shifts by 5.9–42.4% in Asia, 4.8–42.8% in Africa, 24.8–84.2% in Europe, 18.1–65.2% in North America, 1.0–23.0% in South America, and −0.14–16.6% in Oceania (Figure S13 in Supporting Information S1). The frequency of heavy precipitation is projected to change much more quickly for higher percentiles. For instance, the frequency change of the 95th percentile is 4.7–7.7 times that of the 70th percentile in Asia and 0.3–4 timess in Europe.

### 4.2. High Risk Countries and the Unequal Impacts of Extreme Precipitation

Society, government, and market constitute three key dimensions by which to estimate the vulnerability and resilience of a country to natural hazards. Here we use future projections of population exposure and its variability, in conjunction with indicators of socio-economic vulnerability, government ineffectiveness, and economic freedom. Values above 75th percentile are selected for all the indicators and exposure projections to identify high risk countries with less resilience and limited economic recovery capability. Appearing at least twice among the red circles in Figures 5a–5c, Angola, Burkina Faso, DR Congo, Ethiopia, Iran, Malawi, Nepal, Sudan, and Uganda are outstanding in terms of high future exposure. Growing very fast in terms of future population exposure (i.e., the 75th percentile growth rate which is ≥3.74 times larger than the mean), Burundi, Cameroon, Central African Republic, Chad, Djibouti, Lesotho, Liberia, Mali, Papua New Guinea, Rwanda, Sierra Leone,

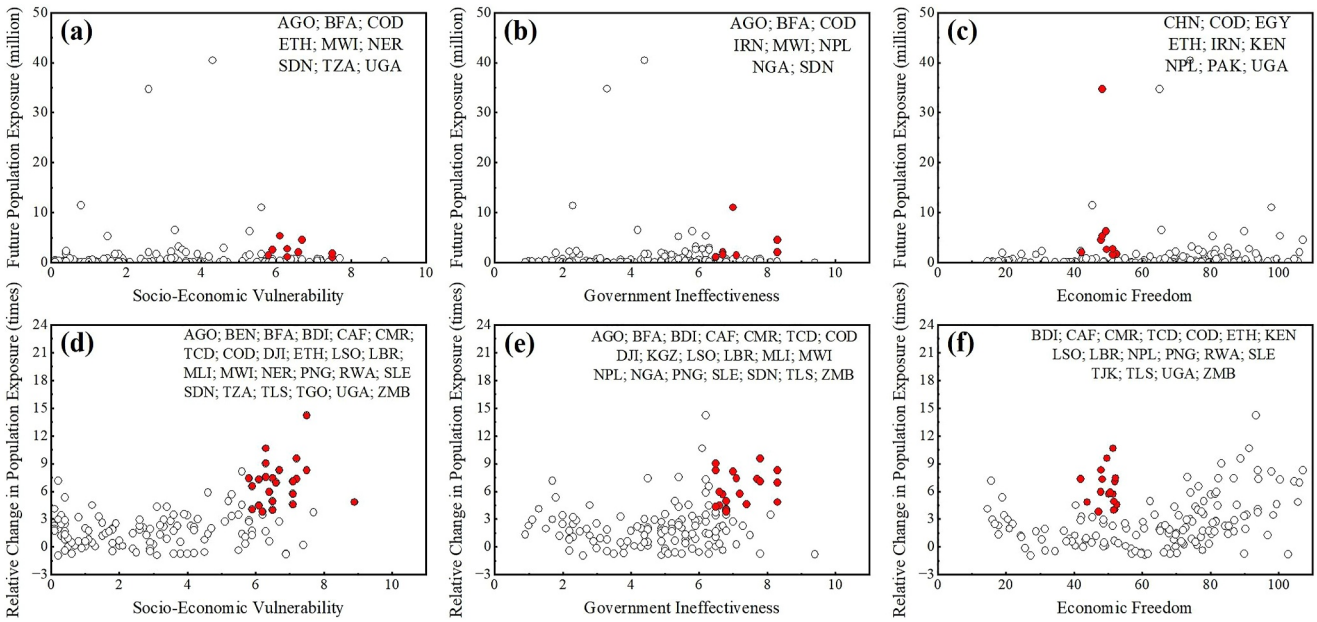


**Figure 5.** Future hotspot countries (red dots) identified by large absolute population exposure (a, b, and (c) or relative change in future population exposure compared to the historical exposure (d), (e), and (f) to extreme precipitation events at the 99th percentile under a medium carbon emission scenario (SSP245) with high socio-economic vulnerability (a) and (d), high government ineffectiveness (b) and (e), or low economic freedom (c) and (f). Three-digit ISO codes for hotspot countries are listed in the upper right corner of each panel (see Table S15 in Supporting Information S1 for the ISO codes).

East Timor, Zambia are likely to become high risk in the long term (i.e., appearing at least twice among the red circles in Figures 5d–5f).

The ability of any given country to cope with natural disasters is also closely related to its degree of sociopolitical stability and social wealth. Here we take the Fragile States Index (FSI) (The Fragile State Index, 2023) as a measure of sociopolitical instability, and GDP as a measure of social wealth, and probe into the relationship between FSI, GDP per capita and indicators of socioeconomic vulnerability, government ineffectiveness, and economic freedom. Strong correlations of FSI with socioeconomic vulnerability ($r^2 = 0.738$, $p < 0.001$) and with government ineffectiveness ($r^2 = 0.807$, $p < 0.001$) are revealed (Figures S14a and S14b in Supporting Information S1), while significant (but relatively weaker) relationships with the economic freedom index ($r^2 = 0.446$, $p < 0.001$) are also found (Figure S14c in Supporting Information S1). Negative semilogarithmic correlations between GDP per capita and socioeconomic vulnerability/government ineffectiveness/economic freedom are also significant ($r^2 = 0.848$ for socioeconomic vulnerability, $r^2 = 0.708$ for government ineffectiveness, and $r^2 = 0.378$ for economic freedom, all at the 0.99 confidence level) (see Figures S14d–S14f in Supporting Information S1). Interestingly, a negative semilogarithmic relationship also exists between per capita GDP and FSI ($r^2 = 0.785$). Hence, it is possible to employ any one of the five investigated measures to assess a country's ability to cope with risks, especially in terms of GDP per capita which is easier to obtain. Combining the 25th percentile of GDP per capita (≤2157 USD) with that of the future population exposure, we identify 88.9%, 62.5%, and 66.7% of the red points in Figures 5a–5c respectively. However, if we alter the choice of GDP percentile just slightly (e.g., 35th percentile), the overlap of high-risk countries with Figures 5a and 5b grows to 100%/87.5%, which supports the appropriateness of using GDP per capita to identify high-risk countries.

## 5. Conclusions

Our research evaluates the socio-economic repercussions of increasing extreme precipitation under future global warming scenarios. Given the considerable uncertainty in climate projections from Earth system models, we develop a robust emergent constraint relationship between the historical and future 99th percentile of extreme precipitation. This new relationship, which is found to be broadly applicable to all global land grid cells, significantly enhances the accuracy of extreme precipitation projections compared to the original CMIP6 model outputs. The study uncovers a widespread increase in the intensity and frequency of future extreme precipitation,

that is expected to significantly affect future populations and GDP. This increase is likely to have serious implications for populous nations, like China and India, as well as politically unstable developing countries. Developed countries with stable or declining populations are also likely to experience rising exposure primarily due to climate change. Countries facing poverty are more vulnerable to the combined effects of climate and socioeconomic changes. Moreover, our research provides nuanced insights into country-specific risk based on socioeconomic vulnerability, governmental capacity, and economic freedom. We reveal unequal impacts of extreme precipitation on countries characterized by low GDP per capita and high sociopolitical instability.

Although our findings highlight a general increase in the intensity and frequency of extreme precipitation across most of the globe, some countries, including Guinea-Bissau, Guyana, Jamaica, and Uruguay exhibit a noteworthy decrease in future precipitation frequency under certain SSPs compared to the historical period. Further, despite our efforts to mitigate uncertainty in precipitation simulations from Earth system models, additional unforeseeable factors affecting population and GDP, such as major natural disasters, wars, and migrations, also contribute to uncertainty, and should be addressed in future research. Besides, HEC framework employed in this work (Bowman et al., 2018) is based on the Gaussian hypothesis which should be tested at the beginning. In particular, climate extremes should be treated with great caution. The distribution of climate extremes over a period usually complies with a Generalized Extreme Value distribution, whereas the distribution across model ensembles is likely to fit the Gaussian distribution. In our study, the Gaussian assumption cannot be denied in 99.26% of all the grids, with the remaining 0.74% fitting other distributions. In such cases, numerical integration is recommended to calculate the conditional expectations and variances in the HEC framework, because the joint probability distributions would be too complicated to deal with analytically.

## Data Availability Statement

Monthly precipitation data from the CMIP6 models under the four emission scenarios of SSP126, SSP245, SSP370, SSP585 for the period 1980–2100 (Coupled Model Intercomparison Project Phase 6, 2019) and from the CMIP5 models under the three emission scenarios of RCP25, RCP45, RCP85 for the period 1900–2100 (Coupled Model Intercomparison Project Phase 5, 2012) were used in the creation of this manuscript. Monthly precipitation observations on which this article is based are available in Beck et al. (2019), Chen et al. (2002), Chen et al. (2008), Xie and Arkin (1997), Xie et al. (2007), and Schneider et al. (2015). The total population, GDP, and GDP per capita, GDP Purchasing Power Parity Conversion Factor, data of countries for the historical were used for access to World Development Indicators from World Bank Group (Population and GDP data, 2022). The total population and GDP data of each country for future projections under four different emission pathways on which this article is based are available in Samir and Lutz (2017), and Dellink et al. (2017). The fragile state index of each country were used for access to The Fragile State Index from The Fund for Peace (The Fragile State Index, 2023). The INFORM-Risk index (Socio-economic Vulnerability and Government Effectiveness) is available for access to INFORM Risk results from European Commission (The INFORM-Risk Index, 2024). The economic freedom index is available for access to Index Of Economic Freedom from The Hertage Foundation (The Economic Freedom Index, 2023). The HEC method processing code and output is available from Liu (2024).

**Acknowledgments**
Financial support is gratefully acknowledged from the National Natural Science Foundation of China (Grant 52079094, 42301018 and 42271219), the Open Fund of State Key Laboratory of Hydraulics and Mountain River Engineering, Sichuan University, China (Grant SKHL2211), UKRI (MR/V022008/1) and NERC (NE/S015728/1). Y.Y. conceptualized the project; Z.L. and Y.Y. wrote the first draft; L.S. and A.G.L.B. edited the draft and contributed ideas; Z.L., Y.C., X.L. and C.M. curated the data; Y.Y., Y.C. and Z.L. designed the methodology; Z.L. performed the analysis and created the visualizations; Y.Y. and Z.Y. supervised the project; Z.Y. and X.L. contributed to the review of the first draft.

## References

Asuero, A. G., Sayago, A., & González, A. G. (2006). The correlation coefficient: An overview. *Critical Reviews in Analytical Chemistry*, *36*(1), 41–59. https://doi.org/10.1080/10408340500526766

Beck, H. E., Wood, E. F., Pan, M., Fisher, C. K., Miralles, D. G., van Dijk, A. I., et al. (2019). MSWEP V2 global 3-hourly 0.1° precipitation: Methodology and quantitative assessment [Dataset]. *Bulletin of the American Meteorological Society*, *100*(3), 473–500. https://doi.org/10.1175/BAMS-D-17-0138.1

Bowman, K. W., Cressie, N., Qu, X., & Hall, A. (2018). A hierarchical statistical framework for emergent constraints: Application to snow-albedo feedback. *Geophysical Research Letters*, *45*(23), 13050–13059. https://doi.org/10.1029/2018GL080082

Brient, F. (2020). Reducing uncertainties in climate projections with emergent constraints: Concepts, examples and prospects. *Advances in Atmospheric Sciences*, *37*, 1–15. https://doi.org/10.1007/s00376-019-9140-8

Brooks, N., Adger, W. N., & Kelly, P. M. (2005). The determinants of vulnerability and adaptive capacity at the national level and the implications for adaptation. *Global Environmental Change*, *15*(2), 151–163. https://doi.org/10.1016/j.gloenvcha.2004.12.006

Chen, H., & Li, H. (2020). Increased population exposure to precipitation extremes under future warmer climates. *Environmental Research Letters*, *15*(3), 034048. https://doi.org/10.1088/1748-9326/ab751f

Chen, H., & Sun, J. (2021). Significant increase of the global population exposure to increased precipitation extremes in the future. *Earth's Future*, *9*(9), e2020EF001941. https://doi.org/10.1029/2020EF001941

Chen, M., Shi, W., Xie, P., Silva, V. B., Kousky, V. E., Wayne Higgins, R., & Janowiak, J. E. (2008). Assessing objective techniques for gauge-based analyses of global daily precipitation [Dataset]. *Journal of Geophysical Research*, *113*(D4). https://doi.org/10.1029/2007JD009132. D04110.

Chen, M., Xie, P., Janowiak, J. E., & Arkin, P. A. (2002). Global land precipitation: A 50-yr monthly analysis based on gauge observations [Dataset]. *Journal of Hydrometeorology*, *3*(3), 249–266. https://doi.org/10.1175/1525-7541(2002)003<0249:GLPAYM>2.0.CO;2

Chen, Z., Zhou, T., Zhang, L., Chen, X., Zhang, W., & Jiang, J. (2020). Global land monsoon precipitation changes in CMIP6 projections. *Geophysical Research Letters*, *47*(14), e2019GL086902. https://doi.org/10.1029/2019GL086902

Coupled Model Intercomparison Project Phase 5. (2012). Program for climate model diagnosis and Intercomparison [Dataset]. *Earth System Grid Federation*. Retrieved from https://esgf-node.llnl.gov/projects/cmip5/

Coupled Model Intercomparison Project Phase 6. (2019). Program for climate model diagnosis and Intercomparison [Dataset]. *Earth System Grid Federation*. Retrieved from https://esgf-node.llnl.gov/projects/cmip6/

Cutter, S. L., Boruff, B. J., & Shirley, W. L. (2003). Social vulnerability to environmental hazards. *Social Science Quarterly*, *84*(2), 242–261. https://doi.org/10.1111/1540-6237.8402002

Das, J., Manikanta, V., & Umamahesh, N. V. (2022). Population exposure to compound extreme events in India under different emission and population scenarios. *Science of the Total Environment*, *806*, 150424. https://doi.org/10.1016/j.scitotenv.2021.150424

de Bruijn, J. A., de Moel, H., Jongman, B., de Ruiter, M. C., Wagemaker, J., & Aerts, J. C. (2019). A global database of historic and real-time flood events based on social media. *Scientific Data*, *6*(1), 311. https://doi.org/10.1038/s41597-019-0326-9

Dellink, R., Chateau, J., Lanzi, E., & Magné, B. (2017). Long-term economic growth projections in the shared socioeconomic pathways [Dataset]. *Global Environmental Change*, *42*, 200–214. https://doi.org/10.1016/j.gloenvcha.2015.06.004

De Silva, M. M. G. T., & Kawasaki, A. (2018). Socioeconomic vulnerability to disaster risk: A case study of flood and drought impact in a rural Sri Lankan community. *Ecological Economics*, *152*, 131–140. https://doi.org/10.1016/j.ecolecon.2018.05.010

Dottori, F., Szewczyk, W., Ciscar, J.-C., Zhao, F., Alfieri, L., Hirabayashi, Y., et al. (2018). Increased human and economic losses from river flooding with anthropogenic warming. *Nature Climate Change*, *8*, 781–786. https://doi.org/10.1038/s41558-018-0257-z

Fatemi, F., Ardalan, A., Aguirre, B., Mansouri, N., & Mohammadfam, I. (2017). Social vulnerability indicators in disasters: Findings from a systematic review. *International Journal of Disaster Risk Reduction*, *22*, 219–227. https://doi.org/10.1016/j.ijdrr.2016.09.006

Forzieri, G., Cescatti, A., Silva, F. B., & Feyen, L. (2017). Increasing risk over time of weather-related hazards to the European population: A data-driven prognostic study. *The Lancet Planetary Health*, *1*(5), e200–e208. https://doi.org/10.1016/s2542-5196(17)30082-7

Gu, L., Yin, J., Gentine, P., Wang, H.-M., Slater, L. J., & Sullivan, S. C. (2023). Large anomalies in future extreme precipitation sensitivity driven by atmospheric dynamics. *Nature Communications*, *14*(1), 3197. https://doi.org/10.1038/s41467-023-39039-7

Hall, A., Cox, P., Huntingford, C., & Klein, S. (2019). Progressing emergent constraints on future climate change. *Nature Climate Change*, *9*(4), 269–278. https://doi.org/10.1038/s41558-019-0436-6

Hallegatte, S., Vogt-Schilb, A., Bangalore, M., & Rozenberg, J. (2016). *Unbreakable: Building the resilience of the poor in the face of natural disasters*. World Bank Publications. https://doi.org/10.1596/978-1-4648-1003-9

International Monetary Fund. (2023). World economic outlook: Navigating global divergences. Retrieved from https://www.imf.org/en/Publications/WEO/Issues/2023/10/10/world-economic-outlook-october-2023

Karunarathne, A. Y., & Lee, G. (2020). Developing a multi-facet social vulnerability measure for flood disasters at the micro-level assessment. *International Journal of Disaster Risk Reduction*, *49*, 101679. https://doi.org/10.1016/j.ijdrr.2020.101679

Liu, Y., Chen, J., Pan, T., Liu, Y., Zhang, Y., Ge, Q., et al. (2020). Global socioeconomic risk of precipitation extremes under climate change. *Earth's Future*, *8*(9), e2019EF001331. https://doi.org/10.1029/2019EF001331

Liu, Z. (2024). The HEC method processing code and output for constrained precipitation extremes reveal unequal future socioeconomic exposure [Dataset]. *Zenodo*. https://doi.org/10.5281/zenodo.14257546

Mesta, C., Cremen, G., & Galasso, C. (2022). Urban growth modelling and social vulnerability assessment for a hazardous Kathmandu Valley. *Scientific Reports*, *12*(1), 6152. https://doi.org/10.1038/s41598-022-09347-x

Murray, V., & Ebi, K. L. (2012). IPCC special report on managing the risks of extreme events and disasters to advance climate change adaptation (SREX). *Journal of Epidemiology & Community Health*, *66*(9), 759–760. https://doi.org/10.1136/jech-2012-201045

Papalexiou, S. M., & Koutsoyiannis, D. (2013). Battle of extreme value distributions: A global survey on extreme daily rainfall. *Water Resources Research*, *49*(1), 187–201. https://doi.org/10.1029/2012WR012557

Papalexiou, S. M., & Montanari, A. (2019). Global and regional increase of precipitation extremes under global warming. *Water Resources Research*, *55*(6), 4901–4914. https://doi.org/10.1029/2018WR024067

Population and GDP data. (2022). World development indicators [Dataset]. World Bank Group. Retrieved from https://data.worldbank.org.cn/indicator/

Rentschler, J., Salhab, M., & Jafino, B. A. (2022). Flood exposure and poverty in 188 countries. *Nature Communications*, *13*(1), 3527. https://doi.org/10.1038/s41467-022-30727-4

Rufat, S., Tate, E., Burton, C. G., & Maroof, A. S. (2015). Social vulnerability to floods: Review of case studies and implications for measurement. *International Journal of Disaster Risk Reduction*, *14*, 470–486. https://doi.org/10.1016/j.ijdrr.2015.09.013

Samir, K. C., & Lutz, W. (2017). The human core of the shared socioeconomic pathways: Population scenarios by age, sex and level of education for all countries to 2100 [Dataset]. *Global Environmental Change*, *42*, 181–192. https://doi.org/10.1016/j.gloenvcha.2014.06.004

Schneider, U., Becker, A., Finger, P., Meyer-Christoffer, A., Rudolf, B., & Ziese, M. (2015). GPCC full data monthly product version 7.0 at 0.5°: Monthly land-surface precipitation from rain-gauges built on GTS-based and historic data [Dataset]. https://doi.org/10.5676/DWD_GPCC/FD_M_V7_050

Shen, L., Wen, J., Zhang, Y., Ullah, S., Cheng, J., & Meng, X. (2022). Changes in population exposure to extreme precipitation in the Yangtze River Delta, China. *Climate Services*, *27*, 100317. https://doi.org/10.1016/j.cliser.2022.100317

Shi, P., Yang, X., Fang, J., Wang, J., Xu, W., & Han, G. (2016). Mapping and ranking global mortality, affected population and GDP loss risks for multiple climatic hazards. *Journal of Geographical Sciences*, *26*(7), 878–888. https://doi.org/10.1007/s11442-016-1304-1

Sohn, B.-J., Yeh, S.-W., Lee, A., & Lau, W. K. (2019). Regulation of atmospheric circulation controlling the tropical Pacific precipitation change in response to $CO_2$ increases. *Nature Communications*, *10*(1), 1108. https://doi.org/10.1038/s41467-019-08913-8

Tanoue, M., Hirabayashi, Y., & Ikeuchi, H. (2016). Global-scale river flood vulnerability in the last 50 years. *Scientific Reports*, *6*(1), 36021. https://doi.org/10.1038/srep36021

Thackeray, C. W., Hall, A., Norris, J., & Chen, D. (2022). Constraining the increased frequency of global precipitation extremes under warming. *Nature Climate Change*, *12*(5), 441–448. https://doi.org/10.1038/s41558-022-01329-1

The Economic Freedom Index. (2023). Index of economic freedom [Dataset]. The Hertage Foundation. Retrieved from https://www.heritage.org/international-economies

The Fragile State Index. (2023). The fragile state index [Dataset]. The Fund for Peace. Retrieved from https://fragilestatesindex.org/global-data/

The INFORM-Risk Index. (2024). The INFORM-risk index [Dataset]. *European Commission*. Retrieved from https://drmkc.jrc.ec.europa.eu/inform-index/INFORM-Risk/Results-and-data/moduleI.d/1782/id/433/controller/Admin/action/Results

United Nations Department of Economic and Social Affairs, Population Division. (2022). World population prospects 2022: Summary of results. Retrieved from https://www.researchgate.net/publication/361944109_World_Population_Prospects_2022_Summary_of_results

Wilks, D. S. (2006). *Statistical methods in the atmospheric sciences* (2nd ed.). Academic Press.

Williamson, M. S., Thackeray, C. W., Cox, P. M., Hall, A., Huntingford, C., & Nijsse, F. J. (2021). Emergent constraints on climate sensitivities. *Reviews of Modern Physics*, *93*(2), 025004. https://doi.org/10.1103/RevModPhys.93.025004

Xie, P., & Arkin, P. A. (1997). Global precipitation: A 17-year monthly analysis based on gauge observations, satellite estimates, and numerical model outputs [Dataset]. *Bulletin of the American Meteorological Society*, *78*(11), 2539–2558. https://doi.org/10.1175/1520-0477(1997)078<2539:GPAYMA>2.0.CO;2

Xie, P., Chen, M., Yang, S., Yatagai, A., Hayasaka, T., Fukushima, Y., & Liu, C. (2007). A gauge-based analysis of daily precipitation over East Asia [Dataset]. *Journal of Hydrometeorology*, *8*(3), 607–626. https://doi.org/10.1175/JHM583.1

Zhang, W., Furtado, K., Zhou, T., Wu, P., & Chen, X. (2022). Constraining extreme precipitation projections using past precipitation variability. *Nature Communications*, *13*(1), 6319. https://doi.org/10.1038/s41467-022-34006-0

Zhang, W., Zhou, T., Zou, L., Zhang, L., & Chen, X. (2018). Reduced exposure to extreme precipitation from 0.5°C less warming in global land monsoon regions. *Nature Communications*, *9*(1), 3153. https://doi.org/10.1038/s41467-018-05633-3

## References From the Supporting Information

Bevington, P. R., & Robinson, D. K. (1992). *Data reduction and error analysis for the physical sciences* (2nd ed.). WCB/McGraw-Hill.

Chai, Y., Yue, Y., Slater, L. J., Yin, J., Borthwick, A. G., Chen, T., & Wang, G. (2022). Constrained CMIP6 projections indicate less warming and a slower increase in water availability across Asia. *Nature Communications*, *13*(1), 4124. https://doi.org/10.1038/s41467-022-31782-7

Taylor, J. R. (1997). *An introduction to error analysis: The study of uncertainties in physical measurements*. University Science Books.